PCCP

Multi-colour circularly polarized luminescence properties of chiral Schiff-base boron difluoride complexes

Journal:	*Physical Chemistry Chemical Physics*
Manuscript ID	CP-ART-04-2022-001861.R1
Article Type:	Paper
Date Submitted by the Author:	09-Jun-2022

Complete List of Authors:	Ikeshita, Masahiro; Nihon University College of Industrial Technology Graduate School of Industrial Technology, Applied Molecular Chemistry Suzuki, Takato; Nihon University College of Industrial Technology Graduate School of Industrial Technology, Applied Molecular Chemistry Matsudaira, Kana; Kindai University, Department of Applied Chemistry Kitahara, Maho; Kindai University Imai, Yoshitane; Kindai University, Department of Applied Chemistry Tsuno, Takashi; Nihon University College of Industrial Technology Graduate School of Industrial Technology, Applied Molecular Chemistry

ARTICLE

Multi-colour circularly polarized luminescence properties of chiral Schiff-base boron difluoride complexes

Received 00th January 20xx,
Accepted 00th January 20xx

DOI: 10.1039/x0xx00000x

Masahiro Ikeshita,*[a] Takato Suzuki,[a] Kana Matsudaira,[b] Maho Kitahara,[b] Yoshitane Imai*[b] and Takashi Tsuno*[a]

A series of chiral Schiff-base boron difluoride complexes was synthesized and their photophysical properties were examined. These complexes showed multi-colour (blue, yellow and red) photoluminescence in solution and in the solid state with good emission quantum yield (Φ) depending on the π-systems of the ligands. The chiral complexes exhibited circularly polarized luminescence (CPL) with an absolute luminescence dissymmetry factor (g_{lum}) of up to the 1.3×10^{-3} in solution and 1.9×10^{-2} in the drop-cast film state. Density functional theory (DFT) and time-dependent (TD) DFT calculations were conducted to further understand the photophysical properties.

Introduction

Circularly polarized luminescence (CPL)[1] is receiving increasing attention in a wide range of fields owing to the huge potential for applications, such as information storage and processing,[2] 3D optical displays,[3] circularly polarized lasers[4] asymmetric synthesis,[5] as well as in biological probes.[6] In the early stages of CPL research, chiral lanthanide complexes[7] have been studied mainly because they exhibit CPL from magnetically allowed and Laporte-forbidden *f-f* transitions with high absolute luminescence dissymmetry factors ($g_{lum} = 2\Delta I/I = 2(I_L - I_R)/(I_L + I_R)$, in which I_L and I_R are the intensity of left- and right-circularly polarized luminescence).[8] In recent years, there has been a growing interest in the study of small organic molecules (SOMs) with CPL activity because of their ease of providing wavelength tunability and external stimuli responsiveness through derivatization.[9] Various examples of CPL-SOMs with chiral frameworks such as helicenes,[10] binaphthyls,[11] cyclophanes,[12] have been reported. However, most of them show CPL with g_{lum} in the range of 10^{-4}–10^{-3}, which is much smaller than that of chiral lanthanide complexes. On the other hand, the CPL of SOM has been found to be enhanced by the emergence of supramolecular chirality in aggregation systems,[13] and it has been reported to increase in various aggregation states such as gels,[14] liquid crystals[15] and films,[16] some of which have g_{lum} exceeding 10^{-1}.[15a-d,16b]

Organoboron complexes have been extensively studied as promising materials for organic light-emitting diodes (OLEDs) owing to their efficient luminescence properties and high carrier mobility.[17] The photophysical properties of such complexes can be tuned mainly through ligand functionalization which influences the colour and emission quantum yield (Φ).[18] CPL can also be induced by incorporating a chiral skeleton into organoboron complexes,[19] and has been applied to circularly polarized organic light-emitting diodes (CP-OLEDs).[20] Among them, boron difluoride complexes have been recognized as promising CPL materials due to their tunable emission and high Φ values. Representative examples of CPL-active boron difluoride complexes with conjugated π-systems including axial chirality,[19i] helical chirality[19j] and planar chirality[19k] are shown in Fig. 1a.

As part of our program aimed at the creation of novel functional materials, we have been investigating luminescent organic and organometallic complexes bearing Schiff-base ligands.[21] Previously, we have reported that phosphorescent Pt(II) complexes with chiral Schiff-base ligands exhibit tunable CPL properties in the poly(methyl methacrylate) (PMMA) f i l m -

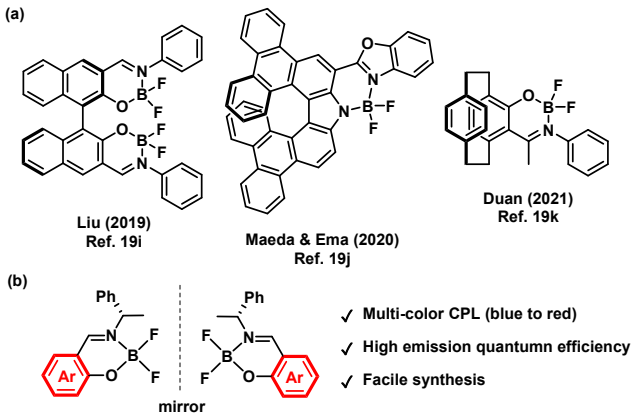

Fig. 1 (a) Previous report of CPL-active boron difluoride complexes

[a] Department of Applied Molecular Chemistry, College of Industrial Technology, Nihon University, Narashino, Chiba 275-8575, Japan. E-mail: ikeshita.masahiro@nihon-u.ac.jp, tsuno.takashi@nihon-u.ac.jp
[b] Department of Applied Chemistry, Faculty of Science and Engineering, Kindai University 3-4-1 Kowakae, Higashi-Osaka, Osaka 577-8502, Japan. E-mail: y-imai@apch.kindai.ac.jp
Electronic Supplementary Information (ESI) available. See DOI: 10.1039/x0xx00000x

with chiral conjugated π-systems. (b) Multi-colour CPL-active boron difluoride complexes studied in this work.

dispersed state.[21b] In the present work, we focused on boron difluoride complexes[22] with chiral (*N*,*O*)-bidentate Schiff-base ligands as CPL emitters (Fig. 1b). These complexes are readily synthesized by the reaction of the corresponding Schiff-base ligands with boron reagents, and their photoluminescence properties can be tuned by modification of the π-systems of the ligands. Notably, the chiral complexes exhibited multi-colour (blue, yellow and red) CPL with moderate g_{lum} values (up to 1.3 × 10^{-3}) in dilute solution state, and their CPL intensities were considerably enhanced by formation of aggregates as in the drop cast film state (up to g_{lum} = 1.9 × 10^{-2}). Theoretical calculations revealed a relationship between their structures and the photophysical properties including CPL ability. Herein we describe the synthesis, structure and photophysical properties of a series of chiral Schiff-base boron difluoride complexes with a focus on their multi-colour CPL properties.

Results and Discussion

Chiral boron difluoride complexes **1a**–**e** were prepared by the reaction of BF_3·OEt_2 with the corresponding optically pure Schiff-base ligands in 1,2-dichloroethane according to the literature procedure (Scheme 1).[22d] Obtained complexes were successfully characterized by ^{1}H and ^{13}C nuclear magnetic resonance (NMR) spectroscopy (Fig. S1–5), infra-red (IR) spectroscopy, high-resolution mass spectrometry (HRMS). Single crystals suitable for X-ray diffraction analysis were obtained by recrystallization from CH_2Cl_2/EtOH and the molecular structures of (*S*)-**1a**–**d** were unambiguously elucidated by X-ray crystallographic analysis. Unfortunately, due to the low crystallinity of compound **1e**, single crystals could not be obtained by recrystallization from any of the organic solvents. The details of the crystal data and the structure refinement are presented in Table S1, including intermolecular interactions (Fig. S9–S12). ORTEP[23] drawings of (*S*)-**1a**–**d** are presented in Fig. 2. In all complexes, boron atoms adopt typical tetrahedral geometry.

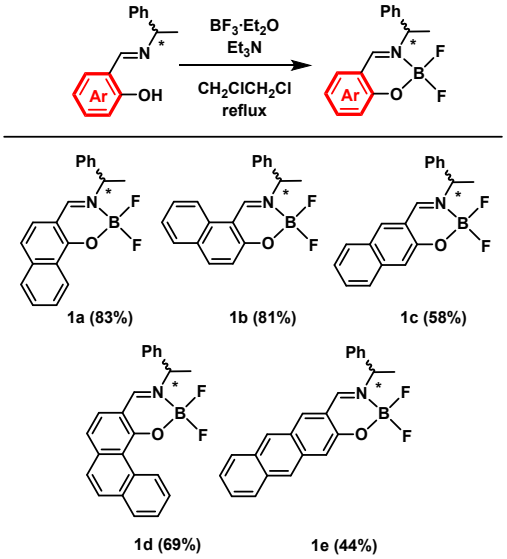

Scheme 1. Synthesis of chiral boron difluoride complexes **1a–e**.

Circular dichroism (CD) spectra of (*R*)-**1a**–**e** and (*S*)-**1a**–**e** were recorded in CH_2Cl_2 solution at room temperature (Fig. 3a and S13). The complexes (*R*)-**1a**–**e** and (*S*)-**1a**–**e** showed mirror image CD spectra, meaning that they are enantiomers (Fig. S13). Complexes (*S*)-**1a**–**d** exhibited a negative Cotton effect around 350–450 nm, which can be assigned to the π–π* transition in the UV-vis spectra showing π–π* bands in the same region (Fig. 3b). On the other hand, complex (*S*)-**1e** showed opposite positive Cotton effect in the same region,

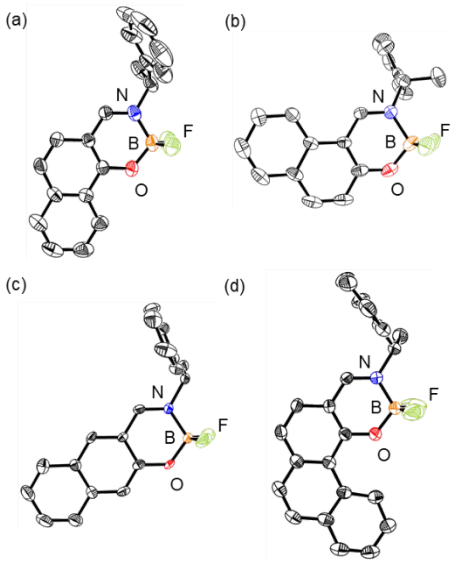

Fig. 2. ORTEP drawings of (a) (*S*)-**1a**, (b) (*S*)-**1b**, (c) (*S*)-**1c** and (d) (*S*)-**1d**. Thermal ellipsoids are shown at 50% probability level. Hydrogen atoms and solvent molecules are omitted for clarity.

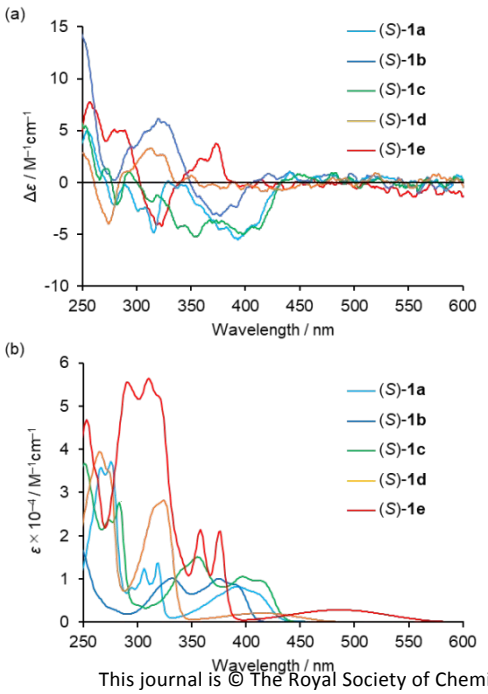

Fig. 3 (a) CD and (b) UV-vis spectra of 2.0 × 10^{-4} M solutions of (*S*)-**1a–e** in CH_2Cl_2 at 298 K.

and the π–π* transition band in the UV-vis spectra was red shifted compared to those of (*S*)-**1a–d**.

The luminescence intensity and colour of the boron complexes were found to vary significantly depending on the π-extension of the ligands. Photophysical data of (*S*)-**1a–e** are presented in Table 1. Quantum efficiencies (Φ) were determined using the absolute method with an integrating sphere accessory. Fig. 4 shows photographs of solutions and crystals of (*S*)-**1a–e** under UV irradiation at 298 K. 2.0×10^{-4} M solutions of (*S*)-**1a–d** in CH_2Cl_2 exhibit intense blue to yellow emission, while (*S*)-**1e** shows weak red emission under the same conditions (Fig. 4a). The low quantum efficiency of (*S*)-**1e** (Φ = 0.01) might be attributed to the increase of non-radiative deactivation in accordance with the energy gap law.[24] Similarly, all complexes exhibit blue to red emission in crystalline state (Fig. 4b). In particular, the crystal of (*S*)-**1a** shows a rather high Φ value exceeding 0.99. The enhanced luminescence quantum yields in the aggregated state, except for (*S*)-**1d**, are considered to be based on the immobilization of molecules through multiple CH-π and H-F interactions observed in the crystal packings (Fig. S9–11).

The emission spectra of the boron complexes measured in CH_2Cl_2 are shown in Fig. 5a, in which the wavelengths of the emission peak maxima (λ_{max}) increase in the order of **1b** (432 nm) < **1a** (460 nm) ≈ **1d** (459 nm) < **1c** (541 nm) < **1e** (623 nm). These results indicate that it is possible to control the emission colour in the range of approximately 200 nm by simple π-extension of the ligands. In addition, the emission peak maxima in the crystalline state show the same trend as in the dilute solution state [**1b**: (λ_{max} = 477 nm) < **1a** (λ_{max} = 483 nm) ≈ **1d**

Fig. 4 Photographs of (a) CH_2Cl_2 solutions (2.0 × 10^{-4} M) and (b) crystals of (*S*)-**1a–e** at 298 K under UV illumination at 365 nm.

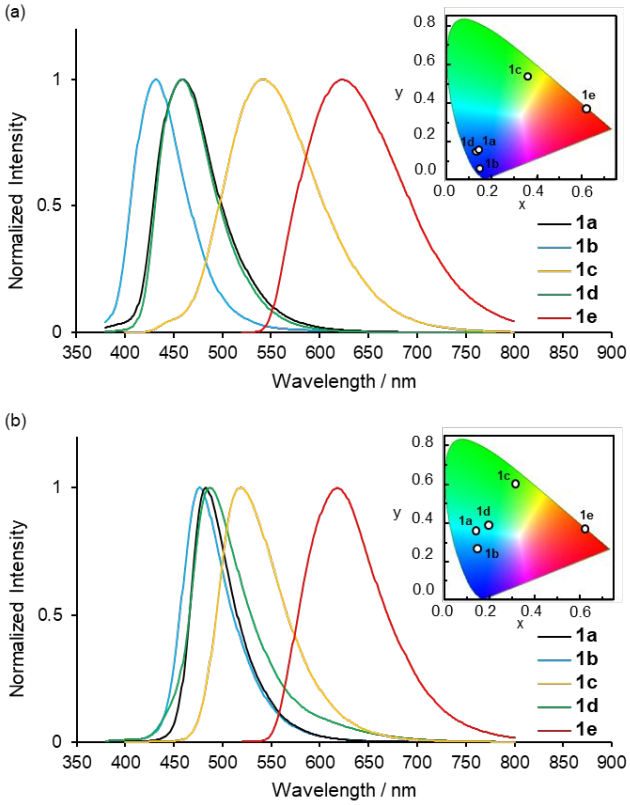

Fig. 5 (a) Normalized emission spectra of (a) CH_2Cl_2 solutions (2.0 × 10^{-4} M) and (b) crystals of (*S*)-**1a–e** (**1a**, **1b**, **1d**: λ_{ex} = 350 nm, **1c**: λ_{ex} = 400 nm, **1e**: λ_{ex} = 480 nm). The insets show the CIE colour coordinates of the emissions.

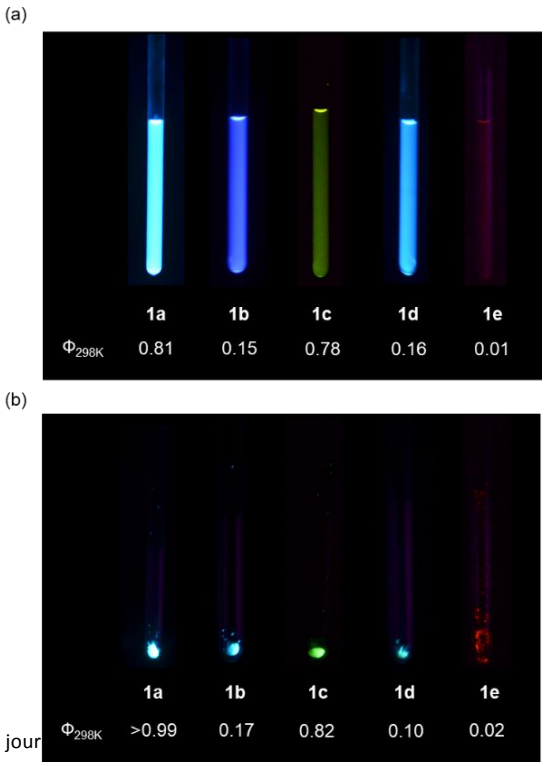

(λ_{max} = 487 nm) < **1c** (λ_{max} = 519 nm) < **1e** (λ_{max} = 618 nm); Table 1]. The CIE colour coordinates plotted on the CIE1930 chromaticity chart (Fig. 5, inset) indicate that the emission colour of (*S*)-**1a–e** varies in each complex.

The CPL spectra of enantiomeric samples of (*R*)-**1a–e** and (*S*)-**1a–e** in dilute CH_2Cl_2 solution showed mirror image spectra (Fig. 6), and emission wavelengths of CPL signals correspond well with those of emission spectra taken under the same measurement conditions (Fig. 5a). In these spectra, complexes (*S*)-**1a–d** exhibited negative CPL sign (Fig. 6a–d), whereas complex (*S*)-**1e** showed opposite positive CPL sign (Fig. 6e). These results indicate that π-extension of the ligands affects the direction of optical polarization, as will be discussed in more detail in a later section. The $|g_{lum}|$ values around the maximum emission wavelength are 6.9 × 10^{-4} (461 nm) for **1a**, 4.3 × 10^{-4} (434 nm) for **1b**, 7.9 × 10^{-4} (541 nm) for **1c**, 6.6 × 10^{-4} (461 nm) for **1d** and 1.3 × 10^{-3} (627 nm) for **1e**, respectively. Fortunately, we successfully prepared clear homogeneous thin films of complexes (*R*)-**1a**,**c** and (*S*)-**1a**,**c** by the drop-cast method and measured their CD and CPL properties. Photophysical data of

film samples of (*S*)-**1a**,**c** are presented in Table 2. In both film samples, mirror-image Cotton effects were observed in their CD spectra (Fig. S14). The CPL and total luminescence spectra measured for (*R*)-**1a**,**c** and (*S*)-**1a**,**c** in the drop-cast film state at 298 K are shown in Fig. 7. The thin films of complexes (*R*)-**1a**,**c** and (*S*)-**1a**,**c** showed intense blue and yellowish green emission

Table 1. Photophysical data for complexes (*S*)-**1a**–**e**.

	Solution[a]					Crystal		
Compound	λ_{abs} [nm]	λ_{max} [nm][b]	Φ[b,c]	CIE (x, y)[b]	g_{lum}[d]	λ_{max} [nm][b]	Φ[b,c]	CIE [x, y][b]
(*S*)-**1a**	392, 411	460	0.81	0.15, 0.14	6.9×10^{-4}	483	>0.99	0.14, 0.35
(*S*)-**1b**	375, 392	432	0.15	0.16, 0.06	4.3×10^{-4}	477	0.17	0.14, 0.26
(*S*)-**1c**	416	541	0.78	0.37, 0.54	7.9×10^{-4}	519	0.82	0.29, 0.61
(*S*)-**1d**	397, 413	459	0.16	0.15, 0.13	6.6×10^{-4}	487	0.10	0.19, 0.39
(*S*)-**1e**	465	623	0.01	0.61, 0.39	1.3×10^{-3}	618	0.02	0.62, 0.39

[a] Data were obtained from a 2.0×10^{-4} M solution in CH_2Cl_2 at 298 K. [b] λ_{ex} = 350 (**1a**, **1b** and **1d**), 400 (**1c**), 480 nm (**1e**). [c] Luminescent quantum efficiencies measured using the absolute method with an integrating sphere. [d] The $|g_{lum}|$ values around emission peak maxima are listed.

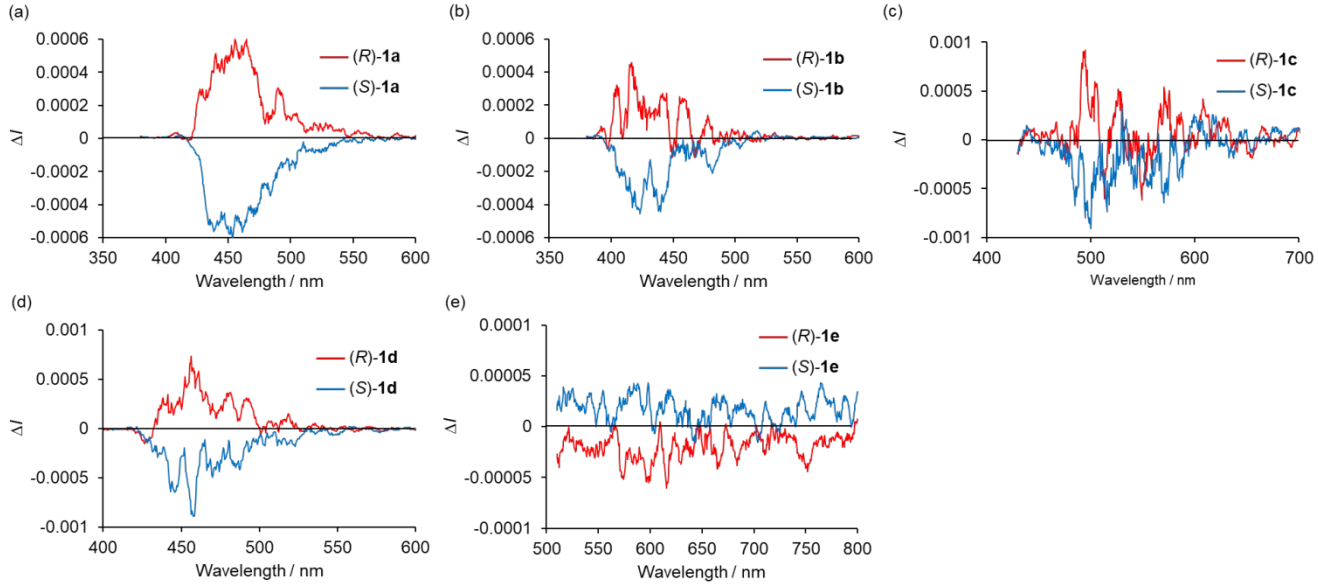

Fig. 6 CPL spectra of 2.0×10^{-4} M solutions of (*R*)- and (*S*)- (a) **1a**, (b) **1b**, (c) **1c**, (d) **1d** and (e) **1e** in CH_2Cl_2 (**1a**, **1b**, **1d**: λ_{ex} = 350 nm, **1c**: λ_{ex} = 400 nm, **1e**: λ_{ex} = 480 nm).

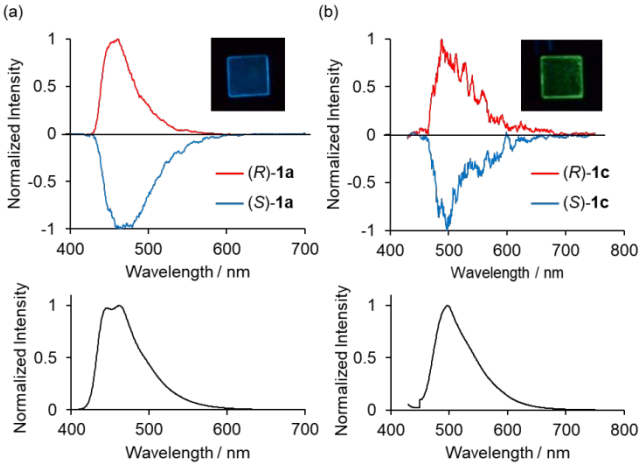

Fig. 7 CPL (upper plot) and total emission (lower plot) of (*R*)- and (*S*)- (a) **1a** and (b) **1c** in drop-cast film state (**1a**: λ_{ex} = 350 nm, **1c**: λ_{ex} = 400 nm). The insets show the photograph of films under UV irradiation (365 nm).

Table 2. Photophysical data for complexes (*S*)-**1a,c** in the drop-cast film state.

Compound	λ_{max} [nm][a]	Φ[a,b]	CIE [x, y][a]	g_{lum}[c]
(*S*)-**1a**	446, 461	0.61	0.15, 0.22	1.9×10^{-2}
(*S*)-**1c**	504	0.40	0.29, 0.55	8.2×10^{-3}

[a] λ_{ex} = 350 (**1a**), 400 (**1c**) nm. [b] Luminescent quantum efficiencies measured using the absolute method with an integrating sphere. [c] The $|g_{lum}|$ values around emission peak maxima are listed.

with high Φ values (**1a**: Φ = 0.61 and **1c**: Φ = 0.40) as in the crystalline state. The emission peak maxima of the films are

446, 461 nm for **1a** and 504 nm for **1c**, which are blue shifted compared with those measured in solution (**1a**: λ_{max} = 460 nm and **1c**: λ_{max} = 541 nm). These results suggest that complexes **1a** and **1c** formed H-type aggregates in the condensed film state.[25] The CPL spectra of both film samples showed clear mirror image signals. Their maximum emission $|g_{lum}|$ values are calculated to be 1.9×10^{-2} (460 nm) for **1a** and 8.2×10^{-3} (488 nm) for **1c**, which is more than 10 times higher than the value measured in solution. This improvement of chirality in the drop-cast films is considered to be due to the emergence of supramolecular chirality caused by H-aggregate formation.

We performed density functional theory (DFT) and time-dependent (TD) DFT calculations on the B3LYP/6-31+G(d,p) level, using the Gaussian 16 program, to clarify the relationship between the molecular structures and the photophysical properties of these complexes. The frontier orbitals of (*S*)-**1a**–**e** and their eigenvalues were estimated by using DFT calculations based on the optimized structure both in the S_0 (ground state) and S_1 (excited state) states (Figs. 8 and S15). The HOMOs of all complexes are principally ligand (π), whereas the LUMOs are in the ligand (π*) (Fig. 8). The energy levels and electronic configurations of the singlet states of these complexes were estimated from TD-DFT calculations (B3LYP/6-31+G(d,p)) (Tables S2 and S3). The major electronic configuration of the S_1 states is the HOMO-to-LUMO transition, which implies that the present emission is principally attributable to π–π* transition. The upward S_0-to-S_1 transition energies were calculated to be 3.22 eV (385 nm) for (*S*)-**1a**, 3.41 eV (364 nm) for (*S*)-**1b**, 2.83 eV (439 nm) for (*S*)-**1c**, 3.15 eV (394 nm) for (*S*)-**1d**, and 2.26 eV (549 nm) for (*S*)-**1e**, which is consistent with the order of the absorption wavelengths of the π–π* transition band for (*S*)-**1a**–**e** observed in CH_2Cl_2 solution [(*S*)-**1b** (375, 392 nm) < (*S*)-**1a** (392, 411 nm) ≈ (*S*)-**1d** (397, 413 nm) < (*S*)-**1c** (416 nm) < (*S*)-**1e** (465 nm); Table 1]. Similarly, the downward S_1-to-S_0 transition energies estimated to be 2.82 eV (440 nm) for (*S*)-**1a**, 3.10 eV (401 nm) for (*S*)-**1b**, 2.16 eV (574 nm) for (*S*)-**1c**, 2.74 eV (453 nm) for (*S*)-**1d** and 1.67 eV (740 nm) for (*S*)-**1e**, are in accord with the emission maxima in CH_2Cl_2.

In order to obtain further insight into the origin of the structure-dependent chiroptical properties observed for (*S*)-**1a**–**e**, we estimated transition dipole moments of upward S_0-to-S_1 and downward S_1-to-S_0 transitions by using TD-DFT calculations (B3LYP/6-31+G(d,p)). The validity of the calculation was confirmed by comparison between theoretical and experimental CD and CPL spectra of (*S*)-**1a**–**e** (Fig. 3a, 7, S16, and S17), showing that the structure-dependent changes in the experimental values are well reproduced by our theoretical simulations. The dissymmetry factors g_{abs} and g_{lum} are calculated with the equation $g = 4(|\mu_e||\mu_m|\cos\theta)/(|\mu_e|^2 + |\mu_m|^2)$, where $|\mu_e|$, $|\mu_m|$ and $\theta_{e,m}$ are the electric transition dipole moments, magnetic transition dipole moments and the angles between two vectors μ_e and μ_m, respectively.[26] Fig. 9 illustrates the electric and magnetic dipole moments $|\mu_e|$ and $|\mu_m|$, calculated for the downward S_1-to-S_0transition of (*S*)-**1a**–**e** in the excited state geometry. The corresponding moments in the ground state are shown in Fig. S18 in the supporting information. In all complexes, calculated g_{lum} values are of the order 10^{-4}–10^{-3} which is consistent with experimental CPL results. The $\theta_{e,m}$ values were obtuse in complexes (*S*)-**1a**–**d**. The $\theta_{e,m}$ values was acute in (*S*)-**1e** despite the fact that all the complexes had the same *S* chirality. These results were consistent with the experimental CPL sign for (*S*)-**1a**–**e**,

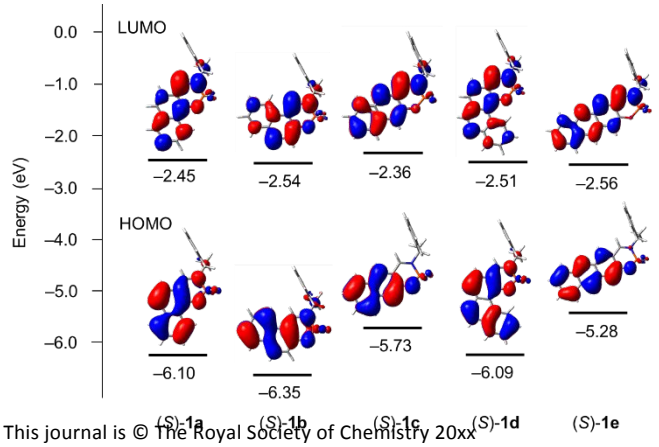

Fig. 8 Molecular orbitals (overhead views) and eigenvalues [eV] for the frontier orbitals of (*S*)-**1a–e** estimated from DFT calculations (B3LYP/6-31+G(d,p)) on the basis of the optimized geometries in the ground states.

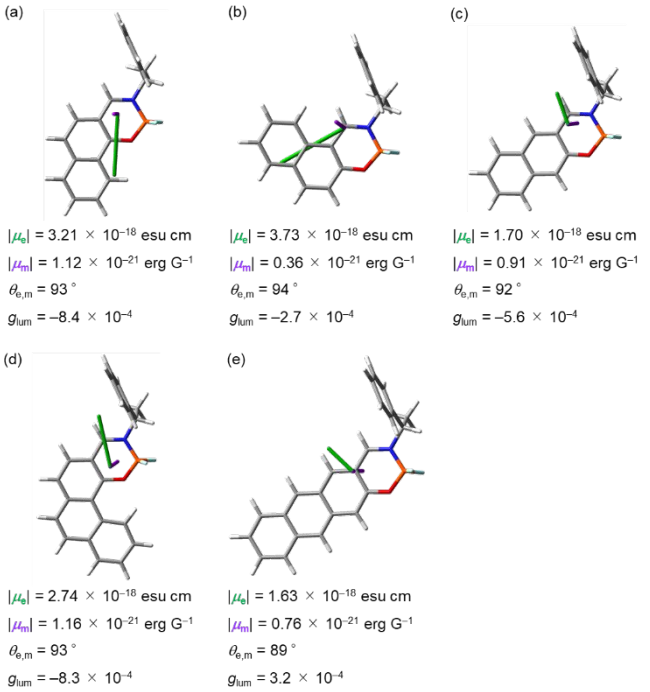

Fig. 9 Electric (μ_e, orange) and magnetic (μ_m, purple) dipole moments of the $S_1 \rightarrow S_0$ transition for (a) (*S*)-**1a**, (b) (*S*)-**1b**, (c) (*S*)-**1c**, (d) (*S*)-**1d** and (e) (*S*)-**1e** calculated at the B3LYP/6-31+G (d,p) level. Calculated values of transition dipole moments ($|\mu_e|$, $|\mu_m|$ and $\theta_{e,m}$) and g_{lum} are given under each structure.

suggesting that modification of the ligands induces a slight difference in the direction of the transition dipole moments leading to the CPL sign inversion.

Conclusions

In summary, we have reported the synthesis and chiroptical properties of chiral Schiff-base difluoride boron complexes. These chiral compounds exhibited multi-colour CPL in the solution state. The CPL intensity was considerably enhanced in the drop-cast film state with g_{lum} value up to 1.9×10^{-2}. DFT and TD-DFT calculations of the structures and electronic configurations of (*S*)-**1a**–**e** revealed the relationship between molecular structure and photophysical properties.

Author Contributions

The project was conceived by Masahiro Ikeshita, who also directed all experiment work, theoretical calculation and wrote the manuscript. Takato Suzuki performed all experimental work except for CPL measurement. Kana Matsudaira and Maho Kitahara measured CPL spectra. Yoshitane Imai and Takashi Tsuno gave constructive guidance for this study. The final version of the manuscript has received the approval of all authors.

Conflicts of interest

There are no conflicts to declare.

Acknowledgements

This work was supported by JSPS KAKENHI (Grant Numbers JP21K20541 (M.I.), JP21K18940 (Y.I.) and JP21K05234 (T.T.)), JST, CREST (Grant Number JPMJCR2001 (Y.I.)), JGC-S SCHOLARSHIP FOUNDATION (M.I.) and Nihon University Industrial Technology Fund for Supporting Young Scholars (M.I.). We gratefully acknowledge Prof. Dr. Henri Brunner (Universität Regensburg) for helpful discussion and comments. We also acknowledge Prof. Dr. Takayoshi Fujii (Nihon University) for measurements of emission properties, and Prof. Dr. Takeshi Naota (Osaka University) and Assoc. Prof. Dr. Shuichi Suzuki (Osaka University) for measurements of HRMS spectrometry.

Notes and references

1 J. P. Riehl and F. S. Richardson, Circularly Polarized Luminescence Spectroscopy, *Chem. Rev.*, 1986, **86**, 1−16.

2 C. Wagenknecht, C.-M. Li, A. Reingruber, X.-H. Bao, A. Goebel, Y.-A. Chen, Q. Zhang, K. Chen and J.-W. Pan, Experimental demonstration of a heralded entanglement source, *Nat. Photonics*, 2010, **4**, 549–552.

3 D.-Y. Kim and Potential Application of Spintronic Light-Emitting Diode to Binocular Vision for Three-Dimensional Display Technology, *J. Korean Phys. Soc.*, 2006, **49**, S505−S508.

4 (a) J. Jiménez, L. Cerdán, F. Moreno, B. L. Maroto, I. García-Moreno, J. L. Lunkley, G. Muller and S. de la Moya, Chiral Organic Dyes Endowed with Circularly Polarized Laser Emission, *J. Phys. Chem. C*, 2017, **121**, 5287−5292; (b) D. Qu, M. Archimi, A. Camposeo, D. Pisignao, E. Zussman, Circularly Polarized Laser with Chiral Nematic Cellulose Nanocrystal Cavity, *ACS Nano*, 2021, **15**, 8753−8760.

5 Y. Inoue, Asymmetric photochemical reactions in solution, *Chem. Rev.*, 1992, **92**, 741−770.

6 M. C. Heffern, L. M. Matosziuk and T. J. Meade, Lanthanide Probes for Bioresponsive Imaging, *Chem. Rev.*, 2014, **114**, 4496−4539.

7 F. Zinna and L. Di Bari, Lanthanide Circularly Polarized Luminescence: Bases and Applications, *Chirality*, 2015, **27**, 1−13.

8 (a) F. S. Richardson and J. P. Riehl, Circularly polarized luminescence spectroscopy, *Chem. Rev.*, 1977, **77**, 773–792; (b) M. Li, W.-B. Lin, L. Fang and C.-F. Chen, Recent Progress on Circularly Polarized Luminescence of Chiral Organic Small Molecules, *Acta Chim. Sinica*, 2017, **75**, 1150−1163; (c) H. Tanaka, Y. Inoue and T. Mori, Circularly Polarized Luminescence and Circular Dichroisms in Small Organic Molecules: Correlation between Excitation and Emission Dissymmetry Factors, *ChemPhotoChem*, 2018, **2**, 386−402.

9 (a) E. M. Sánchez-Carnerero, A. R. Agarrabeitia, F. Moreno, B. L. Maroto, G. Muller, M. J. Ortiz and S. de la Moya, Circularly Polarized Luminescence from Simple Organic Molecules, *Chem. – Eur. J.*, 2015, **21**, 13488−13500; (b) N. Chen and B. Yan, Recent Theoretical and Experimental Progress in Circularly Polarized Luminescence of Small Organic Molecules, *Molecules*, 2018, **23**, 3376; (c) J.-L. Ma, Q. Peng and C.-H. Zhao, Circularly Polarized Luminescence Switching in Small Organic Molecules, *Chem. – Eur. J.*, 2019, **25**, 15441–15454; (d) Y. Imai, Non-classical Circularly Polarized Luminescence of Organic and Organometallic Luminophores, *Chem. Lett.*, 2021, **50**, 1131–1141.

10 (a) J. E. Field, G. Muller, J. P. Riehl and D. Venkataraman, Circularly Polarized Luminescence from Bridged Triarylamine Helicenes, *J. Am. Chem. Soc.*, 2003, **125**, 11808−11809; (b) T. Kaseyama, S. Furumi, X. Zhang, K. Tanaka and M. Takeuchi, Hierarchical Assembly of a Phthalhydrazide-Functionalized Helicene, *Angew. Chem., Int. Ed.* 2011, **50**, 3684−3687; (c) K. Nakamura, S. Furumi, M. Takeuchi, T. Shibuya and K. Tanaka, Enantioselective Synthesis and Enhanced Circularly Polarized Luminescence of S-Shaped Double Azahelicenes, *J. Am. Chem. Soc.*, 2014, **136**, 5555−5558; (d) M. Li, H.-Y. Lu, C. Zhao, L. Shi, Z. Tang and C.-F. Chen, Helical aromatic imide based enantiomers with full-color circularly polarized luminescence, *Chem. Commun.*, 2016, **52**, 9921−9924; (e) H. Tanaka, M. Ikenosako, Y. Kato, M. Fujiki, Y. Inoue and T. Mori, Symmetry-Based Rational Design for Boosting Chiroptical Responses, *Commun. Chem.*, 2018, **1**, 38; (f) W.-L. Zhao, M. Li, H.-Y. Lu and C.-F. Chen, Advances in helicene derivatives with circularly polarized luminescence, *Chem. Commun.*, 2019, **55**, 13793−13803; (g) A. Yubuta, T. Hosokawa, M. Gon, K. Tanaka, Y. Chujo, A. Tsurumaki and K. Kamikawa, Enantioselective Synthesis of Triple Helicenes by Cross-Cyclotrimerization of a Helicenyl Aryne and Alkynes via Dynamic Kinetic Resolution, *J. Am. Chem. Soc.*, 2020, **142**, 10025−10033; (h) H. Kubo, D. Shimizu, T. Hirose and K. Matsuda, Circularly Polarized Luminescence Designed from Molecular Orbitals: A Figure-Eight-Shaped [5]Helicene Dimer with D_2 Symmetry, *Org. Lett.*, 2020, **22**, 9276−9281; (i) H. Kubo, T. Hirose, D. Shimizu and K.

Matsuda, Donor-Acceptor Type [5]Helicene Derivative with Strong Circularly Polarized Luminescence, *Chem. Lett.*, 2021, **50**, 804–807.

11 (a) T. Kawai, K. Kawamura, H. Tsumatori, M. Ishikawa, M. Naito, M. Fujiki and T. Nakashima, Circularly Polarized Luminescence of a Fluorescent Chiral Binaphtylene–Perylenebiscarboxydiimide Dimer, *ChemPhysChem*, 2007, **8**, 1465–1468; (b) T. Kimoto, N. Tajima, M. Fujiki and Y. Imai, Control of Circularly Polarized Luminescence by Using Open- and Closed-Type Binaphthyl Derivatives with the Same Axial Chirality, *Chem. – Asian. J.*, 2012, **7**, 2836–2841; (c) T. Kimoto, T. Amako, N. Tajima, R. Kuroda, M. Fujiki and Y. Imai, Control of Solid-state Circularly Polarized Luminescence of Binaphthyl Organic Fluorophores through Environmental Changes, *Asian J. Org. Chem.*, 2013, **2**, 404–410; (d) K. Nakabayashi, T. Amako, N. Tajima, M. Fujiki and Y. Imai, Nonclassical Dual Control of Circularly Polarized Luminescence Modes of Binaphthyl–Pyrene Organic Fluorophores in Fluidic and Glassy Media, *Chem. Commun.*, 2014, **50**, 13228–13230; (e) K. Takaishi, R. Takehara and T. Ema, Intense Excimer CPL of Pyrenes Linked to a Quaternaphthyl, *Chem. Commun.*, 2018, **54**, 1449–1452; (f) K. Takaishi, K. Iwachido, R. Takehana, M. Uchiyama and T. Ema, Evolving Fluorophores into Circularly Polarized Luminophores with a Chiral Naphthalene Tetramer: Proposal of Excimer Chirality Rule for Circularly Polarized Luminescence, *J. Am. Chem. Soc.*, 2019, **141**, 6185–6190; (g) Y. Nojima, M. Hasegawa, N. Hara, Y. Imai and Y. Mazaki, Stereogenic Cyclic Oligonaphthalenes Displaying Ring Size-Dependent Handedness of Circularly Polarized Luminescence (CPL), *Chem. Commun.*, 2019, **55**, 2749−2752; (h) K. Takaishi, K. Iwachido and T. Ema, Solvent-Induced Sign Inversion of Circularly Polarized Luminescence: Control of Excimer Chirality by Hydrogen Bonding, *J. Am. Chem. Soc.*, 2020, **142**, 1774−1779; (i) Y. Nojima, M. Hasegawa, N. Hara, Y. Imai and Y. Mazaki, Small Figure-Eight Luminophores: Double-Twisted Tethered Cyclic Binaphthyls Boost Circularly Polarized Luminescence, *Chem. – Eur. J.*, 2021, **27**, 5923–5929.

12 (a) Y. Morisaki, M. Gon, T. Sasamori, N. Tokitoh and Y. Chujo, Planar Chiral Tetrasubstituted [2.2]Paracyclophane: Optical Resolution and Functionalization, *J. Am. Chem. Soc.*, 2014, **136**, 3350−3353; (b) S. P. Morcillo, D. Miguel, L. Alvarez de Cienfuegos, J. Justicia, S. Abbate, E. Castiglioni, C. Bour, M. Ribagorda, D. J. Cardenas, J. M. Paredes, L. Crovetto, D. Choquesillo-Lazarte, A. J. Mota, M. C. Carreno, G. Longhi and J. M. Cuerva, Stapled Helical *o*-OPE Foldamers as New circularly Polarized Luminescence Emitters Based on Carbophilic Interactions with Ag(I)-Sensitivity, *Chem. Sci.*, 2016, **7**, 5663–5670; (c) M. Gon, Y. Morisaki and Y. Chujo, Optically Active Phenylethene Dimers Based on Planar Chiral Tetrasubstituted [2.2]Paracyclophane, *Chem. – Eur. J.*, 2017, **23**, 6323−6329; (d) S. Sato, A. Yoshii, S. Takahashi, S. Furumi, M. Takeuchi and H. Isobe, Chiral Intertwined Spirals and Magnetic Transition Dipole Moments Dictated by Cylinder Helicity, *Proc. Nat. Acad. Sci. USA*, 2017, **114**, 13097−13101; (e) P. Renie, A. G. Campaña, L. A. de Cienfuegos, V. Blanco, S. Abbate, A. J. Mota, G. Longhi, D. Miguel and J. M. Cuerva, Chiral Double Stapled *o*-OPEs with Intense Circularly Polarized Luminescence, *Chem. Commun.*, 2019, **55**, 10685–10688; (f) Y. Morisaki and Y. Chujo, Planar Chiral [2.2]Paracyclophanes: Optical Resolution and Transformation to Optically Active π-Stacked Molecules, *Bull. Chem. Soc. Jpn.*, 2019, **92**, 265–274.

13 (a) J. Kumar, T. Nakashima and T. Kawai, Circularly Polarized Luminescence in Chiral Molecules and Supramolecular Assemblies, *J. Phys. Chem. Lett.*, 2015, **6**, 3445–3452; (b) J. Roose, B. Z. Tang and K. S. Wong, Circularly-Polarized Luminescence (CPL) from Chiral AIE Molecules and Macrostructures, *Small*, 2016, **12**, 6495–6512; (c) F. Song, Z. Zhao, Z. Liu, J. W. Y. Lam and B. Z. Tang, Circularly Polarized Luminescence from AIEgens, *J. Mater. Chem. C*, 2020, **8**, 3284–3301.

14 (a) D. Yang, P. Duan, L. Zhang and M. Liu, Chirality and Energy Transfer Amplified Circularly Polarized Luminescence in Composite Nanohelix, *Nat. Commun.*, 2017, **8**, 15727; (b) Y. Sang, P. Duan and M. Liu, Nanotrumpets and Circularly Polarized Luminescent Nanotwists Hierarchically Self-Assembled from an Achiral C_3-Symmetric Ester, *Chem. Commun.* 2018, **54**, 4025–4028; (c) L. Yang, F. Wang, D. Y. Auphedeous and C. Feng, Achiral Isomers Controlled Circularly Polarized Luminescence in Supramolecular Hydrogels, *Nanoscale*, 2019, **11**, 14210–14215.

15 (a) X. Li, Q. Li, Y. Wang, Y. Quan, D. Chen and Y. Cheng, Strong Aggregation-Induced CPL Response Promoted by Chiral Emissive Nematic Liquid Crystals (N*-LCs). *Chem. – Eur. J.*, 2018, **24**, 12607–12612; (b) X. Li, W. Hu, Y. Wang, Y. Quan and Y. Cheng, Strong CPL of Achiral AIE-Active Dyes Induced by Supramolecular Self-Assembly in Chiral Nematic Liquid Crystals (AIE-N*-LCs), *Chem. Commun.*, 2019, **55**, 5179–5182; (c) J. He, K. Bian, N. Li and G. Piao, Generation of Full-Colour and Switchable Circularly Polarized Luminescence from Nonchiral Dyes Assembled in Cholesteric Cellulose Films, *J. Mater. Chem. C*, 2019, **7**, 9278–9283; (d) Y. Li, K. Liu, X. Li, Y. Quan and Y. Cheng, The Amplified Circularly Polarized Luminescence Regulated from D–A Type AIE-Active Chiral Emitters via Liquid Crystals System, *Chem. Commun.*, 2020, **56**, 1117–1120.

16 (a) J. Kumar, T. Nakashima, H. Tsumatori, M. Mori, M. Naito and T. Kawai, Circularly Polarized Luminescence in Supramolecular Assemblies of Chiral Bichromophoric Perylene Bisimides, *Chem. – Eur. J.*, 2013, **19**, 14090–14097; (b) M. Gon, R. Sawada, Y. Morisaki and Y. Chujo, Enhancement and Controlling the Signal of Circularly Polarized Luminescence Based on a Planar Chiral Tetrasubstituted [2.2]Paracyclophane Framework in Aggregation System, *Macromolecules*, 2017, **50**, 1790–1802.

17 (a) F. Jäkle, Advances in the Synthesis of Organoborane Polymers for Optical, Electronic, and Sensory Applications, *Chem. Rev.*, 2010, **110**, 3985–4022; (b) Y.-L. Rao and S. Wang, Four-Coordinate Organoboron Compounds with a π-Conjugated Chelate Ligand for Optoelectronic Applications, *Inorg. Chem.*, 2011, **50**, 12263–12274; (c) G. Wesela-Bauman, P. Ciećwierz, K. Durka, S. Luliński, J. Serwatowski, K. Woźniak, Organoboron Compounds with an 8-Hydroxyquinolato Chelate and Its Derivatives: Substituent Effects on Structures and Luminescence, *Inorg. Chem.*, 2013, **52**, 10846−10859; (d) D. Li, H. Zhang and Y. Wang, Four-Coordinate Organoboron Compounds for Organic Light-Emitting Diodes (OLEDs), *Chem. Soc. Rev.*, 2013, **42**, 8416−8433; (e) D. Frath, J. Massue, G. Ulrich and R. Ziessel, Luminescent Materials: Locking π-Conjugated and Heterocyclic Ligands with Boron(III), *Angew. Chem., Int. Ed.*, 2014, **53**, 2290−2310; (f) M, Gon, K, Tanaka and Y. Chujo, Concept of Excitation-Driven Boron Complexes and Their Applications for Functional Luminescent Materials, *Bull. Chem. Soc. Jpn.*, 2019, **92**, 7–18.

18 (a) Y. Qin, I. Kiburu, S. Shah and F. Jäkle, Luminescence Tuning of Organoboron Quinolates through Substituent Variation at the 5-Position of the Quinolato Moiety, *Org. Lett.*, 2006, **23**, 5227–5230; (b) Z. Zhang, H. Bi, Y. Zhang, D. Yao, H. Gao, Y. Fan, H. Zhang, Y. Wang, Y. Wang, Z. Chen and D. Ma, Luminescent Boron-Contained Ladder-Type π-Conjugated Compounds, *Inorg. Chem.*, 2009, **48**, 7230–7236; (c) D. Li, K. Wang, S. Huang, S. Qu, X. Liu, Q.

Zhu, H. Zhang and Y. Wang, Brightly Fluorescent Red Organic Solids Bearing Boron-Bridged π–Conjugated Skeletons, *J. Mater. Chem.*, 2011, **21**, 15298–15304; (d) M. Yang, I. S. Park and T. Yasuda, Full-Colour, Narrowband, and High-Efficiency Electroluminescence from Boron and Carbazole Embedded Polycyclic Heteroaromatics, *J. Am. Chem. Soc.*, 2020, **142**, 19468−19472; (e) Y. Qi, X. Cao, Y. Zou and C. Yang, Colour-Tunable Tetracoordinated Organoboron Complexes Exhibiting Aggregation-Induced Emission for the Efficient Turn-on Detection of Fluoride Ions, *Mater. Chem. Front.*, 2021, **5**, 2353−2360.

19 (a) H. Maeda, Y. Bando, K. Shimomura, I. Yamada, M. Naito, K. Nobusawa, H. Tsumatori and T. Kawai, Chemical-Stimuli-Controllable Circularly Polarized Luminescence from Anion-Responsive π-Conjugated Molecules, *J. Am. Chem. Soc.*, 2011, **133**, 9266–9269; (b) E. M. Sánchez-Carnerero, F. Moreno, B. L. Maroto, A. R. Agarrabeitia, M. J. Ortiz, B. G. Vo, G. Muller and S. de la Moya, Circularly Polarized Luminescence by Visible-Light Absorption in a Chiral *O*-BODIPY Dye: Unprecedented Design of CPL Organic Molecules from Achiral Chromophores, *J. Am. Chem. Soc.*, 2014, **136**, 3346−3349; (c) S. Zhang, Y. Wang, F. Meng, C. Dai, Y. Cheng and C. Zhu, Circularly Polarized Luminescence of AIE-Active Chiral *O*-BODIPYs Induced via Intramolecular Energy Transfer, *Chem. Commun.*, 2015, **51**, 9014–9017; (d) R. B. Alnoman, S. Rihn, D. C. O'Connor, F. A. Black, B. Costello, P. G. Waddell, W. Clegg, R. D. Peacock, W. Herrebout, J. G. Knight and M. J. Hall, Circularly Polarized Luminescence from Helically Chiral *N*,*N*,*O*,*O*-Boron-Chelated Dipyrromethenes, *Chem. – Eur. J.*, 2016, **22**, 93–96; (e) F. Zinna, T. Bruhn, C. A. Guido, J. Ahrens, M. Bröring, L. Di Bari and G. Pescitelli, Circularly Polarized Luminescence from Axially Chiral BODIPY DYEmers: An Experimental and Computational Study, *Chem. – Eur. J.*, 2016, **22**, 16089–16098; (f) Y. Gobo, M. Yamamura, T. Nakamura and T. Nabeshima, Synthesis and Chiroptical Properties of a Ring-Fused BODIPY with a Skewed Chiral π Skeleton, *Org. Lett.*, 2016, **18**, 2719−2721; (g) R. Clarke, K. L. Ho, A. A. Alsimaree, O. J. Woodford, P. G. Waddell, J. Bogaerts, W. Herrebout, J. G. Knight, R. Pal, T. J. Penfold and M. J. Hall, Circularly Polarised Luminescence from Helically Chiral "Confused" *N*,*N*,*O*,*C*-Boron-Chelated Dipyrromethenes (BODIPYs), *ChemPhotoChem*, 2017, **1**, 513–517; (h) V. G. Jiménez, F. M. F. Santos, S. Castro-Fernández, J. M. Cuerva, P. M. P. Gois, U. Pischel and A. G. Campaña, Circularly Polarized Luminescence of Boronic Acid-Derived Salicylidenehydrazone Complexes Containing Chiral Boron as Stereogenic Unit, *J. Org. Chem.*, 2018, **83**, 14057−14062; (i) Z. Jiang, X. Wang, J. Ma and Z. Liu, Aggregation-Amplified Circularly Polarized Luminescence from Axial Chiral Boron Difluoride Complexes, *Sci. China Chem.*, 2019, **62**, 355–362; (j) C. Maeda, K. Nagahata, T. Shirakawa and T. Ema, Azahelicene-Fused BODIPY Analogues Showing Circularly Polarized Luminescence, *Angew. Chem., Int. Ed.*, 2020, **59**, 7813–7817; (k) K. Li, H. Ji, Z. Yang, W. Duan, Y. Ma, H. Liu, H. Wang and S. Gong, 3D Boranil Complexes with Aggregation-Amplified Circularly Polarized Luminescence, *J. Org. Chem.*, 2021, **86**, 16707−16715; (l) C.-H. Chen and W.-H. Zheng, Planar Chiral Boron Difluoride Complexes Showing Circularly Polarized Luminescence, *Org. Chem. Front.*, 2021, **8**, 6622–6627; (m) W. Duan, H. Ji, Z. Yang, Q. Yao, Y. Huo, X. Ren, J. Zhao and S. Gong, Planar chiral [2.2]paracyclophanyl-based boron fluoride complexes: synthesis, crystal structure and photophysical properties, *Dalton Trans.*, 2021, **50**, 12963–12969.

20 P. Xue, X. Wang, W. Wang, J. Zhang, Z, Wang, J. Jin, C. Zheng, P. Li, G. Xie and R. Chen, Solution-Processable Chiral Boron Complexes for Circularly Polarized Red Thermally Activated Delayed Fluorescent Devices, *ACS Appl. Mater. Interfaces*, 2021, **13**, 47826−47834.

21 (a) M. Ikeshita, M. Ito and T. Naota, Variations in the Solid-State Emissions of Clothespin-Shaped Binuclear *trans*-Bis(salicylaldiminato)platinum(II) with Halogen Functionalities, *Eur. J. Inorg. Chem.*, 2019, 3561−3571; (b) M. Ikeshita, S. Furukawa, T. Ishikawa, K. Matsudaira, Y. Imai and T. Tsuno, Enhancement of Chiroptical Responses of *trans*-Bis[(β-iminomethyl)naphthoxy]platinum(II) Complexes with Distorted Square Planar Coordination Geometry, *ChemistryOpen*, 2022, **11**, e202100277.

22 (a) D. Frath, S. Azizi, G. Ulrich, P. Retailleau and R. Ziessel, Facile Synthesis of Highly Fluorescent *Boranil* Complexes, *Org. Lett.*, 2011, **13**, 3414−3417; (b) G. Wesela-Bauman, M. Urban, S. Luliński, J. Serwatowski and K. Woźniak, Tuning of the Colour and Chemical Stability of Model Boranils: a Strong Effect of Structural Modifications, *Org. Biomol. Chem.*, 2015, **13**, 3268–3279; (c) M. Urban, K. Durka, P. Jankowski and S. Luliński, Highly Fluorescent Red-Light Emitting Bis(boranils) Based on Naphthalene Backbone, *J. Org. Chem.*, 2017, **82**, 8234−8241; (d) P. A. A. M. Vaz, J. Rocha, A. M. S. Silva and S. Guieu, Aggregation-Induced Emission Enhancement of Chiral Boranils, *New J. Chem.*, 2018, **42**, 18166−18171.

23 M. N. Burnett and C. K. Johnson, ORTEP-III: Oak Ridge Thermal Ellipsoid Plot-Program for Crystal Structure Illustrations, Report ORNL-6895, Oak Ridge National Laboratory, Oak Ridge, 1996.

24 J. V. Caspar, T. J. Meyer, Application of the Energy Gap Law to Nonradiative, Excited-State Decay, *J. Phys. Chem.*, 1983, **87**, 952–957.

25 N. J. Hestand and F. C. Spano, Expanded Theory of H- and J-Molecular Aggregates: The Effects of Vibronic Coupling and Intermolecular Charge Transfer, *Chem. Rev.*, 2018, **118**, 7069−7163.

26 L. Rosenfeld, Quantenmechanische Theorie der Natürlichen optischen aktivität von Flüssigkeiten und Gasen, *Z. Phys.* **1929**, *52*, 161−174.